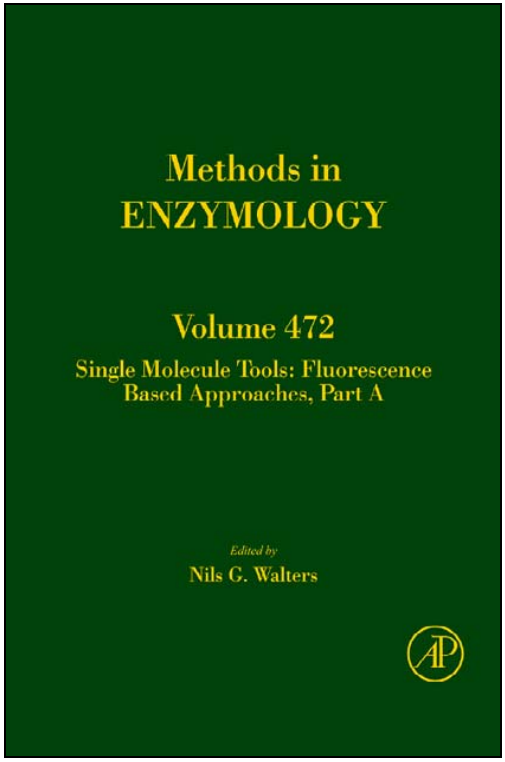

From: Ichiro Amitani, Bian Liu, Christopher C. Dombrowski, Ronald J. Baskin, and Stephen C. Kowalczykowski, Watching Individual Proteins Acting on Single Molecules of DNA
In Nils G. Walters editor: *METHODS IN ENZYMOLOGY,* Vol. 472,
Burlington: Academic Press, 2010, pp.261-291.
ISBN: 978-0-12-374954-3

CHAPTER THIRTEEN

Watching Individual Proteins Acting on Single Molecules of DNA

Ichiro Amitani,[*,†,1] Bian Liu,[*,†,‡,1] Christopher C. Dombrowski,[*,†] Ronald J. Baskin,[†] *and* Stephen C. Kowalczykowski[*,†,‡]

Contents

* Department of Microbiology, University of California, Davis, California, USA
† Department of Molecular and Cellular Biology, University of California, Davis, California, USA
‡ Biophysics Graduate Group, University of California, Davis, California USA
[1] These authors contributed equally to this work.

Methods in Enzymology, Volume 472
ISSN 0076-6879, DOI: 10.1016/S0076-6879(10)72007-3

Abstract

In traditional biochemical experiments, the behavior of individual proteins is obscured by ensemble averaging. To better understand the behavior of proteins that bind to and/or translocate on DNA, we have developed instrumentation that uses optical trapping, microfluidic solution delivery, and fluorescent microscopy to visualize either individual proteins or assemblies of proteins acting on single molecules of DNA. The general experimental design involves attaching a single DNA molecule to a polystyrene microsphere that is then used as a microscopic handle to manipulate individual DNA molecules with a laser trap. Visualization is achieved by fluorescently labeling either the DNA or the protein of interest, followed by direct imaging using high-sensitivity fluorescence microscopy. We describe the sample preparation and instrumentation used to visualize the interaction of individual proteins with single molecules of DNA. As examples, we describe the application of these methods to the study of proteins involved in recombination-mediated DNA repair, a process essential for the maintenance of genomic integrity.

1. Introduction

In traditional ensemble experiments, the behavior of individual proteins is averaged by the obligatory need to study a population of molecules. However, it has become increasingly evident that the analysis of single molecules is not only possible, but that it can reveal novel information about the behavior and function of enzymes (see, e.g., Amitani *et al.*, 2006; Bianco *et al.*, 2001; Galletto *et al.*, 2006; Handa *et al.*, 2005; Nimonkar *et al.*, 2007; Spies *et al.*, 2003, 2007). To better understand the molecular behavior of individual proteins, we have used optical trapping to capture and visualize the action of individual proteins on single molecules of DNA (Bianco *et al.*, 2001). The general experimental design involves attaching a single DNA molecule to a polystyrene microsphere. The microsphere is then used as a handle to manipulate the DNA molecule. Visualization is achieved by using a fluorescence microscope to image fluorescently labeled DNA or protein (Amitani *et al.*, 2006; Bianco *et al.*, 2001; Galletto *et al.*, 2006; Handa *et al.*, 2005, 2009; Hilario *et al.*, 2009). To both extend the DNA and exchange solutions rapidly, we designed and fabricated multichannel microfluidic flow cells that provide parallel paths for different solutions that remain separated by laminar flow (Fig. 13.1) (Bianco *et al.*, 2001; Brewer and

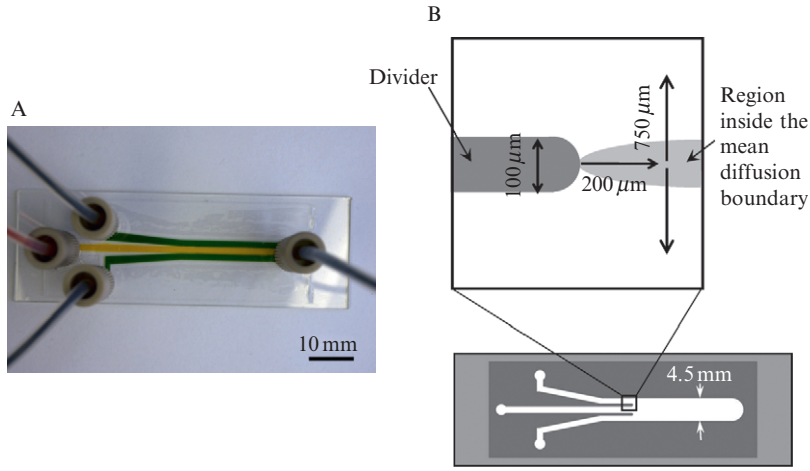

Figure 13.1 Illustration of the three-channel flow cells used in the single-molecule experiments. (A) Photograph of a three-channel flow cell. The flow cell is fabricated using the process described in Section 4.2. To demonstrate the flow path, green dye flows through channels I and III, whereas yellow dye flows through channel 2. (B) Schematic (drawing not to scale) of a three-channel flow cell showing typical dimensions; magnification shows the detail at the end of channel divider. The divider is ~100 μm wide with a semicircular end of radius of ~50 μm. The gray area to the right of the divider illustrates the region inside the mean diffusion length boundary. Experiments are conducted at a point ~200 μm downstream of the divider, ~750 μm into each channel, and ~35 μm from the surface where the effects of diffusion are minimal.

Bianco, 2008). These flow paths are used to introduce the optically trapped DNA to solutions that contain the proteins of interest, or that permit the controlled initiation of enzymatic reactions.

We have applied these methods to the study of proteins involved in recombinational DNA repair, a conserved biological process responsible for the repair of DNA breaks. A DNA double-strand break (DSB) is a lethal type of DNA damage. These breaks are constantly created by many endogenous and exogenous sources in cells. Because an unrepaired DSB often leads to cell death, all organisms have evolved various methods to repair broken DNA. Among them, homologous recombination (HR) is the most accurate method for DSB repair (Kowalczykowski, 2000).

The process of HR consists of three stages. First, the end of a broken double-stranded DNA (dsDNA) molecule is processed by helicase and nuclease to generate a 3′-ended, single-stranded DNA (ssDNA) tail onto which a DNA strand exchange protein self-assembles. Second, this protein–ssDNA complex searches for homology on a donor dsDNA molecule and then catalyzes the pairing and exchange of DNA strands. Finally, the heteroduplex DNA product is resolved (Kowalczykowski, 2000).

In *Escherichia coli*, the RecBCD helicase/nuclease is responsible for the resection of dsDNA ends (Spies and Kowalczykowski, 2005). RecBCD is a bipolar DNA helicase and nuclease (Dillingham and Kowalczykowski, 2008). It unwinds and degrades dsDNA rapidly and processively (Bianco *et al.*, 2001; Roman and Kowalczykowski, 1989). Its biological activities are regulated by an octameric DNA sequence called Chi (*C*rossover *h*otspot *i*nstigator, Chi: 5′-GCTGGTGG-3′) (Dillingham and Kowalczykowski, 2008). Single-molecule analysis uniquely revealed that, upon interaction with Chi, the enzyme pauses for a few seconds, and then it translocates at a reduced rate due to a switch in motor usage (Spies *et al.*, 2003, 2007). The interaction also downregulates the nuclease activity (Dixon and Kowalczykowski, 1993) and switches the polarity of DNA degradation (Anderson and Kowalczykowski, 1997a). These alterations of nuclease activity generate a processed dsDNA ending with a 3′-ssDNA tail (Taylor and Smith, 1995) onto which RecA is loaded by RecBCD to form a nucleoprotein filament (Anderson and Kowalczykowski, 1997b).

DNA strand exchange is catalyzed by RecA in bacteria and Rad51 in eukaryotes (Bianco *et al.*, 1998). Both RecA and Rad51 form a helical nucleoprotein filament on either ssDNA or dsDNA in the presence of ATP. In the filament, RecA/Rad51 occupies 3 nucleotides or base pairs (depending on whether ssDNA or dsDNA is used), and it stretches DNA to 150% of its B-form DNA length (Benson *et al.*, 1994; Chen *et al.*, 2008; Conway *et al.*, 2004; Ogawa *et al.*, 1993; Stasiak *et al.*, 1981). Although the typical active form of RecA/Rad51 is the ssDNA–RecA/Rad51 complex, when assembled on dsDNA, RecA can also promote DNA pairing with ssDNA (Zaitsev and Kowalczykowski, 2000). However, when RecA/Rad51 forms a complex with dsDNA, DNA strand exchange with a RecA/Rad51–ssDNA complex is impeded, resulting in defective recombination (Campbell and Davis, 1999; Sung and Robberson, 1995). Assembly of RecA/Rad51 nucleoprotein filaments occurs by nucleation and growth, a process that was imaged at the single-molecule level (Galletto *et al.*, 2006; Handa *et al.*, 2009; Hilario *et al.*, 2009; Modesti *et al.*, 2007; Prasad *et al.*, 2006; Robertson *et al.*, 2009; van der Heijden *et al.*, 2007). In eukaryotes, the inhibitory Rad51 bound to chromosomes is removed by Rad54 (Solinger *et al.*, 2002), a chromatin-remodeling protein (Alexeev *et al.*, 2003). Rad54 and Tid1, a Rad54 homolog with an important role in meiosis (Klein, 1997; Shinohara *et al.*, 1997), work together with Rad51 (Mazin *et al.*, 2000, 2003; Petukhova *et al.*, 1998; Solinger and Heyer, 2001; Solinger *et al.*, 2001, 2002) and Dmc1, the meiotic Rad51 homolog (Holzen *et al.*, 2006; Shinohara *et al.*, 2000), respectively. Both Rad54 and Tid1 are dsDNA translocases as defined by the direct visualization of their movements on individual DNA molecules (Amitani *et al.*, 2006; Nimonkar *et al.*, 2007; Prasad *et al.*, 2007).

In this chapter, we detail the sample preparation and instrumentation used to visualize the interaction of individual proteins with single molecules of DNA.

2. Preparation of DNA Substrates

2.1. Preparation of biotinylated λ DNA

Bacteriophage λ DNA (New England Biolabs, Ipswich, MA) is biotinylated by ligation to a 3′-biotinylated 12-mer oligonucleotide (5′-GGGCGGCG ACCT-3′ or 5′-AGGTCGCCGCCC-3′, Operon Technologies, Huntsville, AL) that is complementary to one of the cohesive ends of λ DNA (Bianco *et al.*, 2001). In all the subsequent protocols, the pipetting of solutions containing λ DNA should be performed with cut pipette tips to minimize shearing of the DNA.

1. Phosphorylate the oligonucleotide by incubating the oligonucleotide (5 μ*M*) in 50 μl of polynucleotide kinase (PNK) buffer (5 m*M* dithiothreitol (DTT)), 10 m*M* $MgCl_2$, 70 m*M* Tris–HCl (pH 7.6), 1 m*M* ATP, and 0.2 U/μl PNK at 37 °C for 1 h.
2. Stop the reaction by incubation at 75 °C for 10 min.
3. Anneal the phosphorylated oligonucleotide and the λ DNA by preparing a reaction (90 μl) containing 28 ng/μl of λ DNA, 0.56 μ*M* phosphorylated oligonucleotide, and 100 m*M* NaCl.
4. Incubate the reaction at 75 °C for 20 min in a heat block to denature the annealed cohesive ends of the λ DNA.
5. Remove the heat block and place it on the bench to slowly cool the reaction to room temperature (∼2–3 h), and then chill the reaction on ice.
6. Ligate the phosphorylated oligonucleotide to the λ DNA by adding 10 μl of 10× T4 DNA ligase buffer (10 m*M* ATP, 100 m*M* DTT, 100 m*M* $MgCl_2$, 500 m*M* Tris–HCl, pH 7.5) and 1 μl of T4 ligase (400 Units) to the annealing reaction from the previous step.
7. Incubate the reaction at 16 °C overnight or at room temperature for 1 h.
8. Inactivate the ligase by incubating at 75 °C for 10 min.
9. Remove excess oligonucleotide and ATP by filtration through a spin column (MicroSpin S-400 HR, GE Healthcare, Piscataway, NJ).

2.2. Preparation of DNA–bead complexes

DNA–bead complexes are prepared by incubating 1 μl of ∼35 pM streptavidin-coated polystyrene beads (1.0 μm, Bangs Laboratories, Fishers, IN), 1 μl of 100 m*M* $NaHCO_3$ (pH 8.3), and 2 μl of 100 pM biotinylated

λ DNA for 1 h at 37 °C. The ratio of beads to DNA may be varied and optimized for different experiments.

To fluorescently stain the DNA, add 500 μl of sample buffer (see below for experiment-specific recipes) containing 20 n*M* YOYO-1 (Invitrogen, Carlsbad, CA) to the DNA–bead complex and stain in the dark at room temperature for at least 1 h. The dye to DNA (in base pairs) ratio can be altered to vary from 1:1 to 1:5. The sample buffer is degassed for at least 1 h to remove oxygen and to reduce oxygen-mediated photobleaching and cleavage of DNA.

2.3. Preparation of DNA–bead complexes end-labeled with Cy3-labeled antibody

2.3.1. Fluorescent secondary antibody

To visualize the end of a DNA molecule in order to measure its length without the use of a nonspecifically binding dye such as YOYO-1, we attach a fluorescent tag at the free end of the DNA–bead complex (Hilario *et al.*, 2009). To obtain a strong signal for imaging, we fluorescently label a secondary antibody and bind it to a primary antibody that is bound to the end of DNA, which is labeled with digoxigenin (DIG).

1. Exchange the storage solution of donkey antisheep IgG antibody (50 μl, 2 mg/ml, Millipore, Billerica, MA) to a buffer lacking primary amines by using a P30 spin column (850 × *g* for 4 min; Bio-Rad, Hercules, CA) equilibrated with labeling buffer (50 m*M* sodium borate (pH 9.3), 140 m*M* NaCl, and 2.7 m*M* KCl).
2. Add a 20-fold molar excess of Cy3 succinimidyl ester (Cy3-NHS, GE Healthcare) and incubate at room temperature for 1 h in the dark.
3. Remove the unreacted Cy3-NHS with a P30 spin column equilibrated with phosphate buffered saline (PBS; 10 mM Na_2HPO_4, 1.8 mM KH_2PO_4, (pH 7.4), 137 mM NaCl, and 2.7 mM KCl).
4. Determine the Cy3 and antibody concentrations by using the extinction coefficients $\varepsilon_{552} = 1.5\times10^5\ M^{-1}cm^{-1}$ for Cy3, and $\varepsilon_{280} = 1.7 \times 10^5\ M^{-1}cm^{-1}$ for the antibody. The effect of absorption by Cy3 at 280 nm is corrected by: $[\text{antibody}] = (A_{280} - (0.08 \times A_{552}))/1.7 \times 10^5$ (GE Healthcare, Amersham product booklet, "CyDye™ monoreactive NHS Esters").
5. Determine the degree of labeling by calculating the ratio of Cy3 and antibody concentrations. A typical degree of labeling is 6–8 dyes/protein.
6. Store Cy3-antisheep antibody at 4 °C in the dark and use within a few days.

2.3.2. DNA labeled with biotin and digoxigenin (Biotin-λ DNA–DIG)

Bacteriophage λ DNA that is labeled with biotin at one end and DIG at the other end is prepared by attaching a biotin-labeled oligonucleotide and DIG-labeled oligonucleotide to opposite cohesive ends of λ DNA in successive steps.

1. Incubate 750 pM of λ DNA (molecules) with 375 nM of DIG-labeled oligonucleotide (Operon Technologies) in 90 μl of 100 m*M* NaCl at 75 °C for 15 min in a heat block.
2. Remove the heat block and place it on the bench to slowly cool the reaction mixture to room temperature (~2–3 h).
3. Add 10 μl of 10× T4 DNA ligase buffer and T4 DNA ligase to a final concentration of 4 U/μl.
4. Incubate at room temperature for 1 h.
5. Inactivate the DNA ligase at 65 °C for 10 min.
6. Remove unreacted DIG-oligonucleotide with an S-400 spin column (850 × *g* for 5 min) equilibrated with TE buffer (10 mM Tris–HCl (pH 7.5), 1 m*M* EDTA).
7. Add 50-fold molar excess of biotinylated-oligonucleotide and 4 U/μl T4 DNA ligase to DIG-labeled λ DNA.
8. Incubate at room temperature for 1 h.
9. Inactivate the DNA ligase at 65 °C for 10 min.

2.3.3. Binding Cy3-labeled antibody to the DNA–bead complex

DNA–bead complexes that are end-labeled with Cy3-labeled antibody are prepared by binding the sheep anti-DIG antibody to DNA–bead complex, and then binding the Cy3-antisheep secondary antibody to the anti-DIG antibody.

1. Attach the biotin-λ DNA–DIG to streptavidin-coated beads as described in Section 2.2.
2. Add bovine serum albumin (BSA; stock 10 mg/ml) and sheep anti-DIG antibody (stock 200 μg/ml) to final concentrations of 1 mg/ml and 20 μg/ml, respectively.
3. Incubate at room temperature for 2 min.
4. Add Cy3-antisheep IgG antibody to a final concentration of 60 μg/ml. The final volume is ~7 μl.
5. Incubate at room temperature for 2 min.
6. Immediately dilute the Cy3-antibody end-labeled DNA–bead complex into 400 μl of single-molecule buffer (SMB; 40 m*M* Tris–HOAc (pH 8.2), 30 m*M* DTT, and 15% (w/v) sucrose). The final concentration of streptavidin-beads is about 90 f*M*.

3. Preparation of Fluorescent Proteins

3.1. RecBCD labeled with a fluorescent nanoparticle (RecBCD–nanoparticle)

Translocation by individual RecBCD enzyme molecules can be directly visualized by labeling the protein with a fluorescent nanoparticle, which provides a strong and stable fluorescence signal (Handa *et al.*, 2005). Biotinylated RecBCD was purified from an *E. coli* strain that expresses RecD with an N-terminal hexahistidine tag, followed by an amino-acid sequence that directs the biotinylation *in vivo* of a single lysine residue (Handa *et al.*, 2005; Schatz, 1993). To attach the fluorescent nanoparticle:

1. Mix 4.8 μl of the biotinylated RecBCD enzyme (1.22 μM in storage buffer: 20 m*M* Tris–HCl (pH 7.5), 0.1 m*M* EDTA, 0.1 m*M* DTT, 100 m*M* NaCl, and 50% (v/v) glycerol) with 3 μl of a streptavidin-coated fluorescent nanoparticle ($\sim$0.5% solids in 50 m*M* sodium phosphate (pH 7.5), 50 m*M* NaCl, and 5 m*M* sodium azide; 40 nm TransFluoSpheres; excitation 488 nm; emission 645 nm; Molecular Probes, Carlsbad, CA).
2. Incubate for 10 min at 37 °C.

The RecBCD–nanoparticle is subsequently bound to the DNA–bead complex (see below, Section 5.2).

3.2. Rad54/Tid1 labeled with a fluorescent antibody (FITC–Rad54/Tid1)

As an alternative to biotinylation, proteins can be prepared as fusion products; the choice of using a biotinylation tag versus a fusion protein depends on a number of empirical factors, including the efficiency of biotinylation in the organism used for protein expression versus the expression, solubility, and activity of the modified protein. Rather than attaching a streptavidin-coated nanoparticle to the biotin, a fluorescent antibody can be used to label the fusion protein. Yeast Rad54 and Tid1 proteins are purified as a GST fusion product. Consequently, one can directly visualize the translocation of Rad54 or Tid1 by binding a fluorescent antibody to the GST moiety of Rad54 or Tid1 (Amitani *et al.*, 2006; Nimonkar *et al.*, 2007).

1. Prepare DNA–bead complexes as described in Section 2.2.
2. Add DNA translocase to a final concentration of 10 n*M*.
3. Add 670 n*M* FITC-anti-GST antibody (an average degree of labeling of six fluorophores/antibody; RGST-45F-Z, Immunology Consultants Laboratory, Newberg, OR) in PBS containing 0.2% (w/v) BSA. The final volume is $\sim$5 μl.

4. Incubate the mixture at room temperature for 10 min.
5. Immediately dilute the complex into 400 μl of degassed buffer containing 40 m*M* Tris–HOAc (pH 8.2), 30 m*M* DTT, and 15% (w/v) sucrose. The final bead concentration is ~90 f*M*.

3.3. Chemically modified fluorescent RecA or Rad51 proteins ($RecA^{FAM}$/$Rad51^{FAM}$)

RecA and Rad51 can be imaged by the covalent addition of a fluorescent adduct to the N-terminus of the protein (Galletto *et al.*, 2006; Hilario *et al.*, 2009). Chemical modification is performed by coupling 5(6)-carboxyfluorescein succinimidyl ester (FAM-SE, Invitrogen) to the N-terminal amine. Because of the difference in pK_a between N-terminal α-amino group (pK_a~7) and the ε-amino group of lysine (pK_a ~ 10–11), by a judicious adjustment of dye concentration and incubation time, the N-terminal amine of the protein can be relatively specifically labeled (~10^3-fold over other primary amino groups) at near neutral pH to yield products with typically ~1 dye/protein monomer. Here, we describe the protocol to label RecA. The reaction conditions need to be optimized for the protein of interest.

1. The protein is first dialyzed extensively against a solution lacking primary amines (50 m*M* K_2HPO_4/KH_2PO_4 (pH 7.0), 1 *M* NaCl, 0.1 m*M* DTT, and 10% glycerol).
2. Dissolve the FAM-SE in dry DMSO to a stock concentration of ~ 50–75 m*M*. The precise concentration of the stock is determined spectroscopically by making a 1:10,000 dilution into 10 m*M* Tris–HCl (pH 9.0) and using an extinction coefficient of $7.8 \times 10^4\ M^{-1}\ cm^{-1}$ at 492 nm.
3. Add a 12-fold molar excess of FAM-SE to typically 80–100 μM RecA (~500 μl) and incubate at 4 °C for 4 h in the dark.
4. Stop the reaction by adding Tris–HCl (pH 7.5) to a final concentration of 50 m*M*.
5. Remove unreacted fluorescein (FAM) by using a Bio-Gel P10 (Bio-Rad) column (1 cm × 16 cm).
6. Dialyze the sample against storage buffer (20 m*M* Tris–HCl (pH7.5), 0.1 m*M* EDTA, 0.5 m*M* DTT, 10% (v/v) glycerol).
7. Determine the RecA and FAM concentrations by measuring the absorption at 280 and 492 nm using the extinction coefficients of $\varepsilon_{280} = 2.7 \times 10^4\ M^{-1}\ cm^{-1}$ for RecA and $\varepsilon_{492} = 7.8 \times 10^4\ M^{-1}\ cm^{-1}$ for fluorescein measured at pH 9.
8. Determine the degree of labeling by calculating the ratio of FAM and RecA concentrations. A correction factor ($C_F = A_{280}/A_{492}$) of 0.32 measured for the free dye in the absence of protein is used to account for the absorption of FAM at 280 nm using the following calculation:

$A_{RecA} = A_{280} - C_F \times A_{492}$. The correction factor may be sensitive to buffer conditions, specifically pH. It is recommended that the C_F provided by the manufacturer is verified experimentally.

The chemical modification of human Rad51 (at 50–60 μM) is performed in buffer containing 50 mM KH_2PO_4 (pH 7.1), 200 mM KCl, 0.1 mM DTT, and 25% (v/v) glycerol, using 20-fold molar excess of FAM, reacted for 6 h at 4 °C. The labeled protein is stored in storage buffer (50 mM Tris–HOAc (pH 7.5), 200 mM KCl, 1 mM DTT, 0.1 mM EDTA, 50% glycerol) (Hilario et al., 2009).

4. Instrument

4.1. Flow cell design

Single-molecule reactions are carried out in multi-channel flow cells. The photograph of a three-channel flow cell is shown in Fig. 13.1A. Flow cells are designed to ensure laminar flow and to minimize mixing of solutions from different channels (Figs. 13.1 and 13.2). Channel dividers are 100 μm in width with an approximately semicircular end of 10–100 μm, depending on the manufacturing process. Each flow channel is 1.5 mm in width and 70 μm in depth. Fluid flow in this geometry is at a very low Reynolds number (<1) and laminar. The velocity field is a Poiseuille flow with a parabolic profile; maximum velocity is midway between the top and bottom of the flow cell, and zero velocity at the top and bottom surfaces.

To ensure that experiments are conducted in regions where diffusion from adjacent channels is minimal, trapping must occur at a position that is downstream of the confluence and away from the boundary between flow channels. The mean diffusion distance, x, of a solute can be calculated as

$$\langle x^2 \rangle = 2Dt \tag{13.1}$$

$$D = \frac{k_B T}{6\pi\eta a} \tag{13.2}$$

Here, D is the diffusion rate of the solute, k_B is the Boltzmann constant, T is the absolute temperature, η is the viscosity of the solution, and a is the radius of the diffusing particle. The mean diffusion distance provides a good approximation of the boundary where little diffusion between the channels has occurred. However, the absolute concentration will contain solute or ligand from adjacent channels some distance past the mean diffusion boundary. Fig. 13.2 shows a simulation of a solute concentration for two typical solutes (Mg^{2+} and ATP) in our flow cells under nominal conditions. The

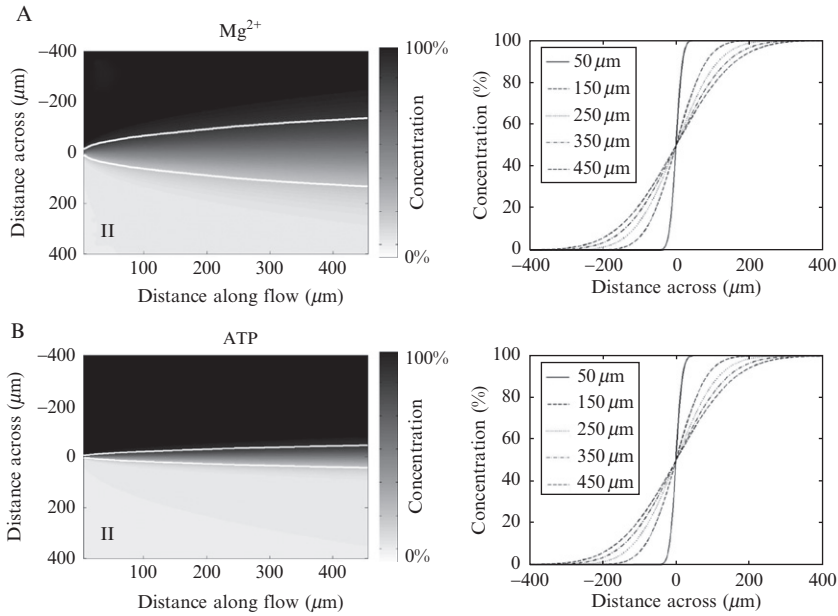

Figure 13.2 The calculated concentrations of Mg^{2+}, $D = 10^{-5}$ cm^2/s (A, left panel), and ATP, $D = 10^{-6}$ cm^2/s (B, left panel) as a function of position for diffusion from channel I into channel II. The flow cell has the same dimensions as described in Fig. 13.1, and the flow rate, v, is 50 μm/s from left to right; the end of the divider is at the origin of the plot. The cross section of concentration as a function of the distance downstream of the flow cell is also shown (right panels). The solid white line in the left panels indicates the mean diffusion distance of the solute from and into each channel. The calculations were performed in MATLAB (MathWorks).

simulations are based on the exact solution of Fick's equation for one-dimensional diffusion in a pipe.

Typically, a flow velocity of 100–200 μm/s is used (Fig. 13.1B). Experiments are conducted by optically trapping $\sim$200 μm downstream of the dividers into the flow cell, halfway between the top and bottom surfaces ($\sim$35 μm), and halfway into the channel ($\sim$750 μm). This position ensures that experiments are conducted in a region where the local solution concentration is identical to the bulk concentration within a channel.

4.2. Flow cell fabrication

Several methods have been used to make multichannel flow cells (for a review, see Brewer and Bianco, 2008). MMR Technologies employs a dry etching technique to create channels on a glass slide; the coverslip is attached to the slide by melting powdered glass at 660 °C (MMR Technologies,

Mountain View, CA). Another way to construct flow cells is to use chemically amplified, negative-tone, epoxy-based photoresists. A multichannel flow cell ~70 μm deep can be made using the following process (Fig. 13.3).

1. Prepare a mask on a chrome borosilicate photomask using standard lithography techniques.
2. Drill inlet and outlet holes on a glass coverslip or slide for either an upright or an inverted microscope using diamond grinding bit (model 750, Dremel, WI). The glass should be submerged under water during grinding.
3. Clean the coverslip and slide with hot piranha treatment (96% H_2SO_4:30% H_2O_2 = 3:1 (v/v)).
4. Spin coat KMPR 1050 photoresist (MicroChem Corp., Newton, MA) onto the slide at 2000 rpm for 30 s.
5. Soft bake at 100 °C for 20 min.
6. Expose the coated slide with 365 nm light using the prepared mask on a Karl-Suss MA4 Mask Aligner (Karl Suss America, Inc., Waterbury Center, VT).
7. Bake at 100 °C for 4 min.
8. Remove unexposed photoresist in SU-8 developer (MicroChem Corp.) for 4 min with slow shaking.

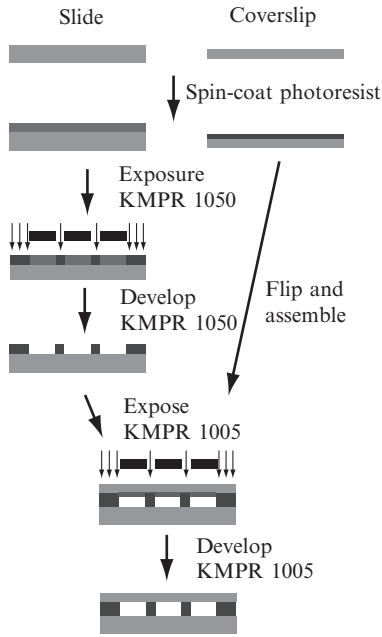

Figure 13.3 Flow diagram for the microfabrication of a three-channel flow cell (see text for details).

9. Spin coat KMPR 1005 photoresist (MicroChem Corp.) onto the coverslip at 1600 rpm for 30 s.
10. Put both the coverslip and the slide on a hotplate at 60 °C with the KMPR-coated side facing up.
11. Flip the coverslip onto the slide. Carefully align the coverslip and the slide before dropping the coverslip onto the slide.
12. Increase the hotplate temperature to 90 °C. When the temperature reaches 90 °C, gently touch the coverslip so that the coverslip and the slide bond together, then decrease the temperature to 60 °C.
13. Expose the coverslip and slide assembly to 365 nm light using the mask prepared in step 1 on a Karl-Suss MA4 Mask Aligner.
14. Bake at 100 °C on a hotplate for 1 min.
15. Remove unexposed photoresist in SU-8 developer by running the developer through the channels with vacuum.
16. Attach machined connectors (P-770-01, Upchurch Scientific, Oak Harbor, WA) to the coverslip at the holes using epoxy.

An alternative way to make flow cells is to use thermobond film or Parafilm:

1. Drill inlet and outlet holes (~1 mm diameter) on the coverslip or slide, depending on the type of microscope (upright or inverted) used.
2. Place either thermobond film (Thermobond film 668EG, 2.5 mil (62 μm), 3 *M*, St. Paul, MN) or Parafilm on the slide. Cut the desired pattern using a razor blade.
3. Place a coverslip on top of the spacer.
4. Place the assembly on a heat block at ~150 °C for 20–30 s. Gently press the coverslip so that the slide and the coverslip bond evenly.
5. Using either a handheld grinding tool or a razor blade, create a V-shape at one end of a short piece (1–2 cm) of PEEK tubing (Upchurch Scientific).
6. Attach the V-shaped end of the PEEK tubing into the holes and glue it using epoxy. Care must be taken not to block the channels.

4.3. Microscope with laser trap and microfluidic system

The laser-trap systems are constructed around a Nikon Eclipse E400 or a Nikon TE2000U microscope (Nikon, Tokyo, Japan). Schematics of the instruments are shown in Figs. 13.4 and 13.5. A brief description of the components follows.

4.3.1. Single optical trap imaging system

A high-pressure mercury lamp (USHIO America, Inc., Cypress, CA) and Y-FL 4-cube Epi-Fluorescence (Nikon) attachment are used for illumination. Images are captured using a high-sensitivity electron bombardment

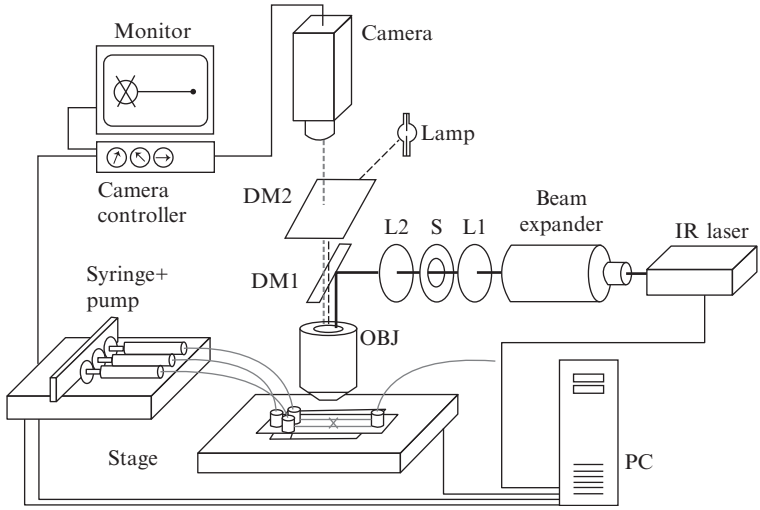

Figure 13.4 Schematic diagram of the microscope, optical trap, and flow cell. The trapping IR *laser* initially passes through a 20× *beam expander*, and is then further collimated and steered by lenses L1 and L2 an electronic shutter (S) is in-between. A high-pass IR dichroic mirror (DM1) directs laser beam into the objective (OBJ). The flow cell is mounted on an *x–y* translocation *stage* that is controlled by a computer (PC) solutions are delivered to the flow cell using a multisyringe pump. A high-pressure mercury arc *lamp* is used for illumination (fluorescence and bright field). A second dichroic mirror (DM2) is used to image the fluorescent protein–DNA–bead complex onto an electron bombardment *camera*; the real-time image is displayed on a *monitor*.

CCD camera (EB-CCD C7190, Hamamatsu Photonics, Hamamatsu City, Japan), recorded on video tape, and subsequently digitalized using an LG-3 frame grabber at 30 frame/s (Scion Corporation, Frederick, MD). The optical trap is created by focusing a 1064 nm laser (Nd:YVO_4, 6 W max, J-series power supply, Spectra Physics, Mountain View, CA) through a high numerical aperture (NA) objective (100×/1.3 oil DICH, Nikon). A high NA objective is necessary to create an intensity gradient sufficiently large to form the trap (Neuman and Block, 2004). The laser is expanded with a 20× beam expander (HB-20XAR.33, Newport, Irvine, CA) to fill the back aperture of the objective. The laser is collimated and aligned using two lenses with the same focal length forming a 1× telescope. The laser is reflected along the optical axis of the microscope by means of a low-pass dichroic mirror (DM) placed between the objective and the fluorescence cube.

Experiments are carried out in a multichannel microfluidic flow cell held on a computer controlled motorized stage (MS-2000, Applied Scientific Instruments, Eugene, OR) mounted on the microscope. The solutions are introduced into the flow cell by a syringe pump with multiple syringes

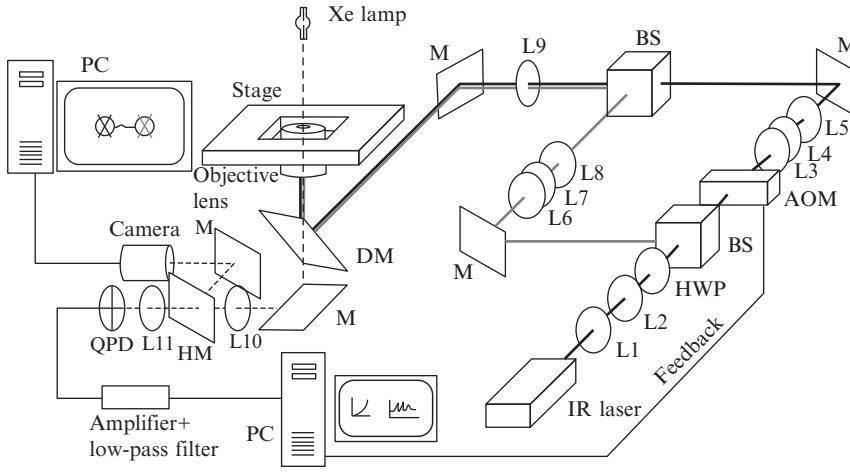

Figure 13.5 Schematic diagram for a dual laser-trap microscope. Lenses L1 and L2 initially collimate and expand the laser. The first beam path (black line) passes through an AOM which is imaged on the back aperture of the *objective lens* by lenses L3, L4, L5, and L9. The second beam path (gray line) is reflected off a movable mirror which is imaged onto the back aperture of the objective by lenses L6, L7, L8, and L9. The image from the objective (dashed line) is split between a *camera* that images the fluorescent protein–DNA–bead complex, and a quadrant photodiode (QPD) for position detection of the bead in the first trap by means of a half-mirror (HM). The signal from the QPD passes through an amplifier and a low-pass filter before being processed by a PC which uses the information to control the AOM, thus providing feedback control on the position of the first trap with nm resolution. Mirrors (M) and beam splitters (BS) serve to direct the beam path. A dichroic mirror (DM) is used to direct the trapping lasers into the objective and to pass light from the Xenon lamp to the camera and QPD; the real-time image is displayed on a monitor. Lenses L10 and L11 image the trapped bead onto the camera and QPD.

(KD Scientific, Hollston, MA). PEEK tubing (Upchurch Scientific) is used to connect the syringes to the flow cell. The microfluidic system permits the imaging of protein–DNA complexes on a single molecule of flow-stretched DNA; it also enables the rapid movement of the sample to the different buffers in the channels of the flow cell. The position of the stage and hence the flow cell, is controlled using a custom-built program. Because the translation speed of the motorized sample stage is typically 0.5–1 mm/s, and the distance being moved to the adjacent flow channel is 0.7–1.5 mm, the time required to move between solution channels is 1–2 s.

4.3.2. Dual optical trap imaging system

For force measurements, a double laser-trap system is constructed around a TE2000U microscope (Fig. 13.5). An infrared laser (Nd:YVO_4, 6 W max, J-series power supply, Spectra Physics) beam is passed through lenses L1 and

L2 ($f = 6$, 12 mm, respectively) serving as a collimator. The beam is then passed through a half-wave plate (HWP) and a polarizing beam splitter (BS) creating two separate beam paths. The first beam is steered with an acoustic optical modulator (AOM) for force feedback. The first beam path is then magnified with lenses L3, L4, L5, and L9 ($f = 75$, 25, 25, 800 mm, respectively) to fill the back aperture of the microscope objective. Similarly, the second path is magnified with lenses L6, L7, L8, and L9 ($f = 75$, 25, 25, 800 mm, respectively) to fill the back aperture of the microscope objective. The laser-trap strength can be up to 0.4 pN/nm, but heating at high-power settings can be a problem. A dichroic mirror (DM) is used to direct the trapping lasers into the objective and to pass light from the Xenon lamp to the camera and quadrant photodiode (QPD). The florescent image of the trapped protein–DNA–bead complex is focused onto a CCD camera (iXon+, Andor) via the objective through another BS. One of the trapped beads is also imaged onto the QPD (S1557-03, Hamamatsu) to provide precise high-bandwidth information about its position. Signals are digitized (PCI6052E, National Instruments) and processed with software written in LabView (LabView 6.1, National Instruments). The position data from the QPD controls the deflection angle of the AOM allowing for feedback between the bead position and the trap position. This arrangement permits the movement of one optical trap relative to the other. The total moveable range of the AOM is 2.4 μm, but the linear range is limited to ± 200 nm.

4.4. Temperature determination and control

To achieve reliable trapping in a flow field, laser power in the range of several hundred milliwatts (mW) is used. Water has a measurable absorption at the near-infrared wavelength typically used for an optical trap ($\lambda = 1064$ nm). Consequently, the effect of local heating on sample temperature is an important consideration. Different ways of estimating the temperature in an optical trap have been reported (Celliers and Conia, 2000; Liu *et al.*, 1995; Peterman *et al.*, 2003). We adapted the methods using fluorescence, and we measured temperature based on the thermal quenching of rhodamine B (RhB) fluorescence (Karstens and Kobs, 1980; Romano *et al.*, 1989). The temperature measurement is carried out using a customized sample chamber (Fig. 13.6). This chamber is constructed as described in Section 4.3. A thermocouple (model CHAL-002, Omega Engineering, Stamford, CT) is placed in the middle of the channel before assembling the coverslip and slide.

4.4.1. Temperature determination

The following procedure is used to measure temperature based on the fluorescence intensity measurements of RhB relative to Alexa-488.

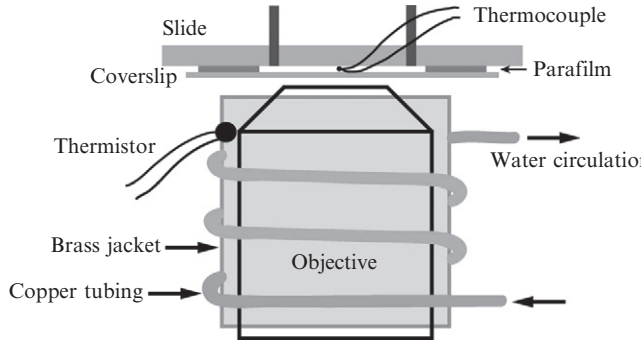

Figure 13.6 Schematic illustration of the components used for temperature measurement and control. *Top*: the flow cell used for temperature determination is made of a glass slide, a coverslip, and a layer of Parafilm sandwiched in between. A thermocouple is placed inside the channel. *Bottom*: an illustration of the temperature controller (side view; not to scale).

1. Construct a flow cell as described in Figure 13.6, Section 4.3. Place a thermocouple (model CHAL-002, Omega Engineering, Stamford, CT) in the middle of the channel before assembling the coverslip and slide.
2. Fill the flow cell with 10× dye solution (10 μM RhB (Wako Pure Chemical Industries, Ltd.) and 15 μM Alexa-488 (Invitrogen) in TE buffer) and incubate at 40 °C overnight to coat the flow cell.
3. Replace the 10× dye solution with degassed 1× dye solution. Seal the outlets using Parafilm.
4. Set the flow cell temperature using either a thermoelectric microscope slide temperature controller (BC-100, 20/20 technologies, Wilmington, NC) or an objective jacket (see next Section 4.4.3). Wait for at least 30 min for the system to equilibrate.
5. Select a region (~5 μm × 10 μm) around the trapping position and record the fluorescence images of RhB and Alexa-488 with the appropriate filter sets (Ethidium Bromide set 41006 and Blue set 11001v2; Chroma Technology Corp., Rockingham, VT).
6. Repeat steps 4 and 5 for at least four different temperatures. These measurements are used to relate the fluorescence intensity to temperature (see below).
7. Turn on the IR laser, set the desired power, and wait for about 30 min.
8. Select the same region as in step 4. Record the fluorescence images of RhB and Alexa-488.
9. Change the IR laser power and repeat steps 7 and 8.
10. Replace the dye solution with TE buffer. Record the background fluorescence images of RhB and Alexa-488.

11. Remove the flow cell and the objective lens. Measure the laser power at the back aperture of the objective. Calculate the power delivered to the focus using the infrared transmission coefficient of the objective used (60% for the objective used) (Neuman and Block, 2004).

To determine the average temperature around the focus, the fluorescence images are analyzed with ImageJ (NIH; http://rsb.info.nih.gov/ij/). A calibration curve of relative fluorescent intensity versus temperature is generated for the data acquired in the absence of trapping laser power. The temperature at any given laser power setting is then obtained from the calibration curve:

1. Calculate the relative fluorescence intensity, $I_r(T)$, at each temperature, T, measured above in the absence of IR irradiation using

$$I_r(T) = (I_R - I_{R,BG})/(I_A - I_{A,BG}) \tag{13.3}$$

where I_R and I_A are the average fluorescence intensity of RhB and Alexa-488 at temperature T, respectively; $I_{R,BG}$ and $I_{A,BG}$ are the average background fluorescence intensities using RhB and Alexa-488 filter sets, respectively.

2. Normalize the relative intensity $I_r(T)$ to an arbitrary reference temperature, T_0 (e.g., 25 °C), using

$$r(T) = I_r(T)/I_r(T_0) \tag{13.4}$$

where $r(T)$ is the normalized intensity ratio.

3. Determine the constant, α, in the empirical linear relationship (Kato *et al.*, 1999) (Fig. 13.7A):

$$r(T) = 1 - \alpha(T - T_0) \tag{13.5}$$

4. The temperature at any given IR laser power is given by

$$T = \frac{1 - r}{\alpha} + T_0 \tag{13.6}$$

where r is the observed intensity ratio normalized to the reference temperature at that given IR laser power.

5. The temperature change for any given IR laser power is

$$\Delta T = T - T_0 = \frac{1 - r}{\alpha} \tag{13.7}$$

For our instrument, the IR laser-induced temperature change is about 1.2 °C/100 mW of laser power delivered at the focus (Fig. 13.7B).

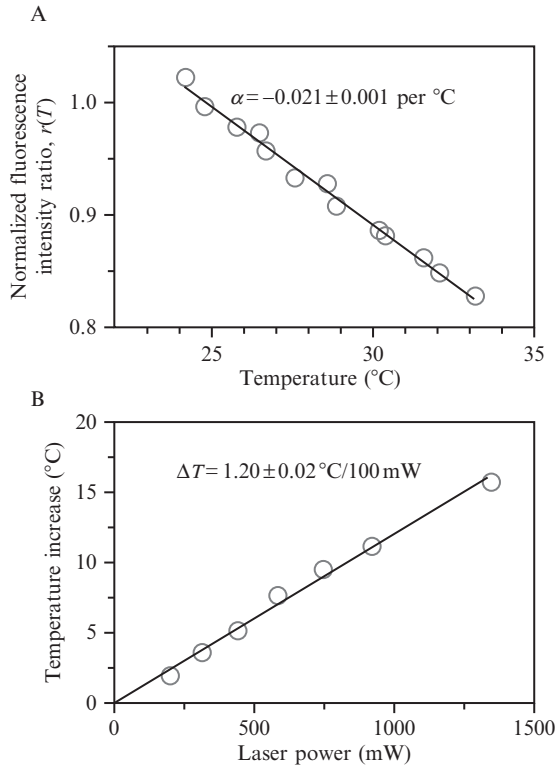

Figure 13.7 Measurement of IR laser-induced temperature changes. (A) Relative fluorescence as a function of temperature. The ratio of the background-corrected fluorescence of RhB and Alexa-488 is normalized to that at 25 °C. The relative fluorescence intensity decreases 2% per °C increase. (B) Relationship between induced temperature change and the IR laser power delivered at the focus, at a starting temperature of 25 °C.

4.4.2. Temperature gradient around the trap center

In an optical trap, hundreds of mW of laser power are focused on a micrometer-sized spot. The temperature gradient caused by such localized heating is another concern. To experimentally determine this gradient, the fluorescence images of RhB and Alexa-488 are recorded as described in Section 4.4.1. The images are then analyzed using the same procedure as in Section 4.4.1 except that the images are analyzed on a pixel-by-pixel basis, using the intensity measured at each pixel, instead of the average fluorescence intensity of the region. The constant α (Eq. (13.5)) for each pixel is then calculated from the normalized intensity ratios $r(T)$ (Kato *et al.*, 1999; Romano *et al.*, 1989). The temperature distribution in a selected region of our instrument is shown in Fig. 13.8A. The temperature gradient in the absence of flow is about 0.06 °C/μm (Fig. 13.8B).

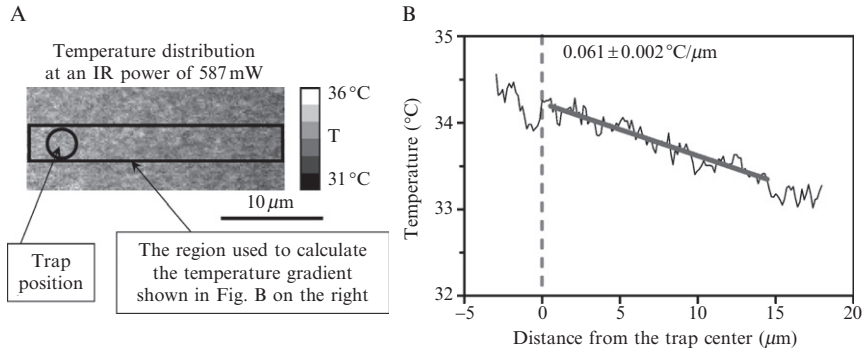

Figure 13.8 **Thermal gradient in a flow cell due to infrared heating by an optical trap. (A) Example showing the measured temperature distribution in an optical trap with an IR laser power of 587 mW when the temperature is set at a starting temperature of 24 °C using only the microscope slide temperature controller. The circle indicates the position of the trap. The rectangle indicates the region where the temperature shown in B is measured. (B) Plot of the temperature distribution in the horizontal direction of the region shown in (A). Black: measured temperature; gray: linear fitting from 0.5 to 14.5 μm away from the trap center. Linear fitting gives a temperature gradient of 0.06 °C/μm.**

4.4.3. Temperature control

Due to the need to use an oil-immersion lens, we discovered that the temperature of the flow cell is largely determined by the heat transfer from the objective to the sample. Although a thermoelectric microscope slide temperature controller (BC-100, 20/20 Technologies, Wilmington, NC) can be used for temperatures within a few degrees of ambient and for low power IR laser settings, a thermostated objective lens is a more effective regulator of sample temperature (Mao *et al.*, 2005). A water circulation system is used to control the temperature of the oil-immersion objective (Fig. 13.6). The temperature control module consists of a brass jacket that fits onto the objective lens and copper tubing that is soldered for several turns around the jacket. The temperature of the objective is controlled by circulating temperature-controlled water from a water bath (Isotemp Refrigerated Circulator, Model 910, Fisher Scientific, Pittsburgh, PA) through the tubing. Water circulation does not perturb the optical trapping. This temperature control module can control the temperature of the sample from 15 to 45 °C and reduces laser-induced heating by 60%.

5. Single-Molecule Imaging of Proteins on DNA

A general single-molecule experiment includes the following steps: (1) prepare DNA attached to the polystyrene bead, either with or without a bound protein of interest; (2) introduce appropriate solutions into different

channels of the multichannel flow cell; (3) capture a DNA–bead complex in the optical trap; and (4) move it into other channels containing ligands or proteins of interest.

5.1. Unwinding of DNA by a single RecBCD enzyme

To visualize DNA unwinding by an individual RecBCD enzyme (Bianco *et al.*, 2001; Spies *et al.*, 2003), a complex of RecBCD enzyme bound to YOYO-1-stained DNA is optically trapped in the absence of ATP; the complex is then moved into the reaction channel, which contains ATP, to initiate DNA unwinding. DNA unwinding and RecBCD enzyme translocation are monitored as a shortening of the DNA length.

1. Prepare a sample buffer containing 45 m*M* $NaHCO_3$ (pH 8.3), 20% sucrose (w/v), and 50 m*M* DTT; degas for at least 1 h.
2. Wash all syringes, tubing, and flow cell with 500 μl of 0.5% (v/v) of blocking reagent (B-10710, Molecular Probes, Carlsbad, CA) in sample buffer using a flow rate of 800 μl/h.
3. Prepare DNA–bead complexes as described in Section 2.2.
4. Add 500 μl of 20 n*M* YOYO-1 in sample buffer to the DNA–bead reaction.
5. Incubate in the dark at room temperature for at least 1 h.
6. Add $Mg(OAc)_2$ and RecBCD to the stained DNA–bead complex at final concentrations of 2 m*M* and 50 n*M*; immediately transfer to the sample syringe (first channel).
7. Prepare 500 μl reaction solution containing the sample buffer supplemented with 2 m*M* $Mg(OAc)_2$ and ATP at various concentrations; load the reaction syringe (second channel).
8. Trap a RecBCD–DNA–bead complex in the first channel.
9. Immediately move the trapped complex to the second channel to start the reaction. The unwinding of dsDNA is manifested by the shorting of the YOYO-1-labeled DNA (Fig. 13.9A and B).

5.2. Direct observation of RecBCD–nanoparticle translocation

Another way to visualize translocation by individual RecBCD enzyme molecules is to attach a fluorescent nanoparticle to RecBCD (Handa *et al.*, 2005).

1. Prepare a sample buffer containing 45 m*M* $NaHCO_3$ (pH 8.3), 20% (w/v) sucrose, and 50 m*M* DTT; degas for at least 1 h.
2. Wash all syringes, tubing, and flow cell with 500 μl of 0.5% (v/v) of blocking reagent (B-10710, Molecular Probes) in sample buffer using a flow rate of 800 μl/h.

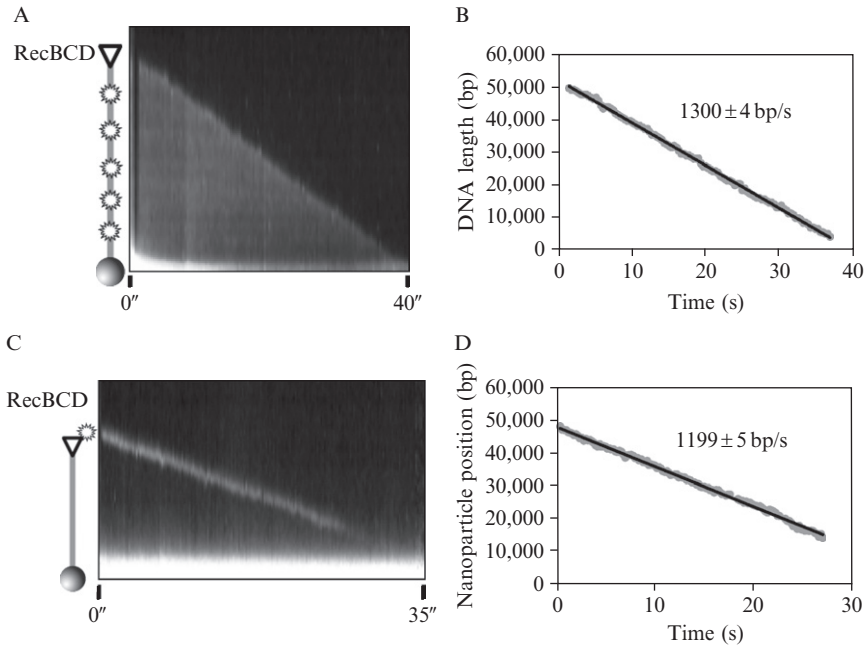

Figure 13.9 RecBCD translocating through, and unwinding, an individual λ DNA molecule. (A) Kymograph showing a YOYO-1 stained λ dsDNA molecule being unwound by a RecBCD molecule bound to the free DNA end. The drawing to the left of the kymograph depicts the optically trapped bead–YOYO-1-DNA–RecBCD complex. (B) Plot of DNA length versus time. Black line shows the fit to a straight line. (C) Kymograph showing translocation by a fluorescent nanoparticle-labeled RecBCD molecule on λ dsDNA. The drawing on the left side of the kymograph depicts the optically trapped bead–DNA–RecBCD–nanoparticle complex. (D) Plot of the position of the RecBCD molecule, indicated by the nanoparticle, versus time. The black line shows the fit to a straight line. Note that the difference in unwinding rates in (B) and (D) is not due to a difference in the techniques, but rather reflects the intrinsic heterogeneity of individual RecBCD enzyme behavior.

3. Prepare DNA–bead complexes as described in Section 2.2.
4. Label biotinylated RecBCD using a fluorescent nanoparticle as described in Section 3.1.
5. Add the DNA–bead complex and 2 m*M* $Mg(OAc)_2$ to the biotinylated RecBCD–nanoparticle complex, and incubate the resulting mixture for 2 min.
6. Dilute the nanoparticle–RecBCD–DNA–bead complex with 400 μl of degassed sample buffer supplemented with 2 m*M* $Mg(OAc)_2$ and 0.5% (v/v) blocking solution (B-10710, Molecular Probes); transfer to the sample syringe (first channel).

7. Load the reaction syringe with the reaction buffer consisting of 1 m*M* ATP, 2 m*M* $Mg(OAc)_2$, and 0.5% (v/v) blocking solution in sample buffer (second channel).
8. Trap a nanoparticle–RecBCD–DNA–bead complex in the first channel.
9. Immediately move the trapped complex to the second channel. The fluorescent particle is seen to move toward the trapped bead as RecBCD translocates on the DNA (Fig. 13.9C and D).

5.3. Rad54/Tid1 translocation

To observe Rad54/Tid1 translocation (Amitani *et al.*, 2006; Nimonkar *et al.*, 2007), a two-channel flow cell is used. Figure 13.10A shows a schematic illustration of the translocation assay, a kymograph showing

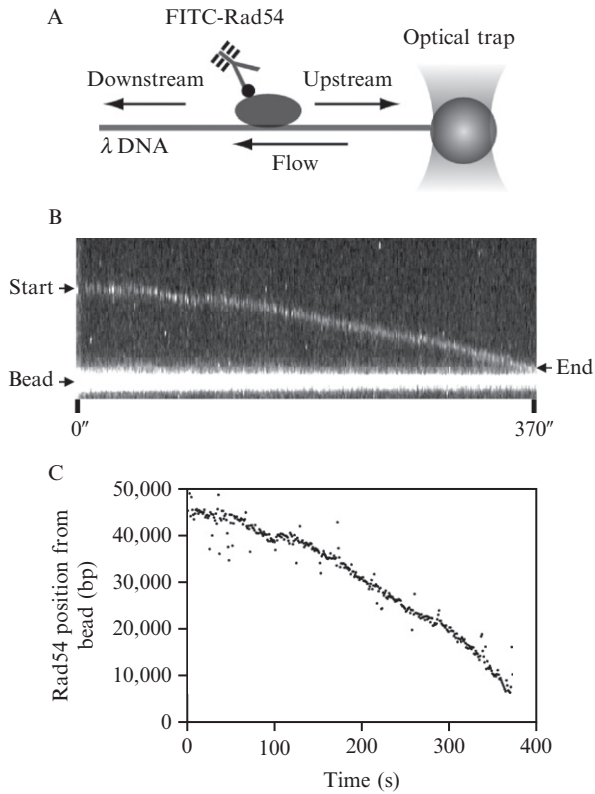

Figure 13.10 Rad54 translocating on a single dsDNA molecule. (A) Schematic illustration of the optically trapped λ DNA–bead complex with a bound FITC–Rad54 complex. (B) Kymographs depicting upstream translocation (in the direction opposite to flow) of Rad54 on the dsDNA. (C) Plot of FITC–Rad54 position relative to the bead versus time.

translocation by Rad54 labeled with FITC-antibody (Fig. 13.10B), and a graph of FITC–Rad54 position as a function of time (Fig. 13.10C).

1. To reduce nonspecific binding, the syringe, tubing, and flow cell are incubated with 0.5 mg/ml of BSA in 50 m*M* Tris–HOAc (pH 7.5) at room temperature for 15 min, then rinsed with a 10-fold volume of 50 m*M* Tris–HOAc (pH 7.5).
2. Prepare FITC–Rad54/Tid1–DNA–bead complexes as described in Section 3.2.
3. Load 400 μl of the FITC–Rad51/Tid1–DNA–bead complex (typically 90 f*M*) in 40 m*M* Tris–HOAc (pH 8.2), 30 m*M* DTT, and 15% (w/v) sucrose into the first channel.
4. Load 400 μl of solution containing 1 m*M* ATP, 2 m*M* $Mg(OAc)_2$, 40 m*M* Tris–HOAc (pH 8.2), 30 m*M* DTT, and 15% (w/v) sucrose into the second channel.
5. Trap a FITC–Rad54/Tid1–DNA–bead complex in the optical trap in the first channel.
6. Move the complex to the second channel containing the ATP to initiate translocation. The fluorescently tagged Rad54 is seen to translocate toward the trapped bead (upstream) (Fig. 13.10B and C) or away from the trapped bead (downstream).

5.4. Real-time Rad51 assembly

To detect the assembly of Rad51 in real time, a two-channel flow cell is used (Hilario *et al.*, 2009). Rad51 assembly can be measured by monitoring the increase in the length of fluorescently end-labeled DNA. A kymograph is shown in Fig. 13.11A; Fig. 13.11B shows a graph of DNA length versus time.

1. To reduce nonspecific binding, the syringe, tubing, and flow cell are washed at 800 μl/h with 0.5 mg/ml of BSA and 0.5 mg/ml casein in 50 m*M* Tris–HOAc (pH 7.5) at room temperature for 1 h, followed by a rinse with sample buffer for 1 h.
2. Prepare Cy3–DNA–bead complexes as described in Section 2.3.
3. Load 400 μl of solution containing Cy3–DNA–bead complexes (about 90 f*M*), 40 m*M* Tris–HOAc (pH 8.2), 30 m*M* DTT, and 15% (w/v) sucrose into the first channel.
4. Load 400 μl of solution containing Rad51, 10 m*M* $Mg(OAc)_2$, 2 m*M* ATP, 40 m*M* Tris–HOAc (pH 7.5), 30 m*M* DTT, and 15% (w/v) sucrose into the second channel. The Rad51 concentration can be varied from 50 n*M* to 1 μ*M*.
5. Trap a Cy3–DNA–bead complex in the first channel.
6. Move the complex to the second channel to initiate Rad51 assembly.

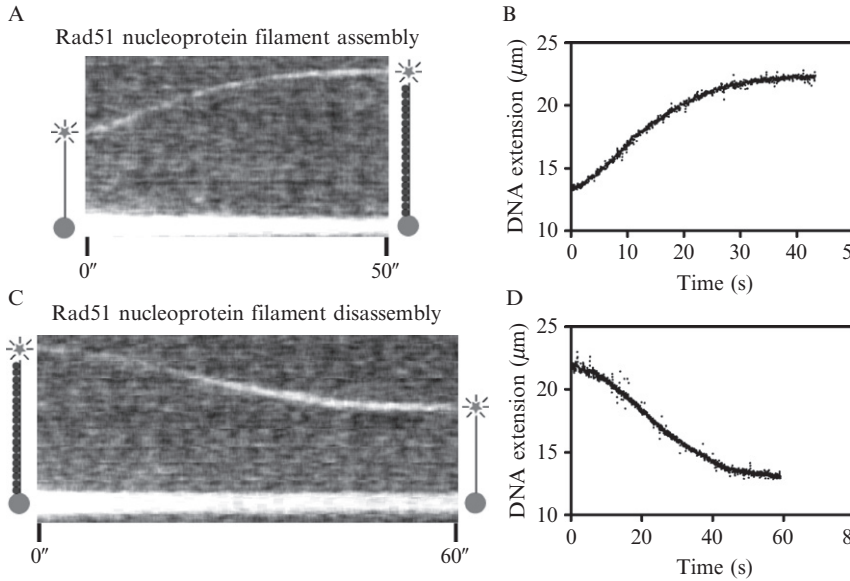

Figure 13.11 Rad51 assembling onto, and dissociating from, a single dsDNA molecule. (A) Kymograph of Rad51 assembly on Cy3-end-labeled λ DNA. The schematic on the left side of kymograph depicts the optically trapped bead, initial position of Cy3-end-label of the DNA (star), and DNA (solid line); the schematic on the right side depicts the extended Rad51 nucleoprotein filament. DNA length is measured from the center of the bead to the Cy3-end-label. (B) Plot of DNA length versus time for the assembly of Rad51 on DNA analyzed using two-dimensional Gaussian fitting of the end-label position. (C) Kymograph of Rad51 disassembly from Cy3-end-labeled λ DNA. The schematic on the left side of kymograph depicts the optically trapped bead, initial position of Cy3-end-label of the DNA (star), Rad51 (filled circles), and DNA (solid line). (D) Plot of DNA length versus time for the disassembly of Rad51 from DNA.

5.5. Real-time Rad51 disassembly

To visualize the disassembly of a Rad51 nucleoprotein filament in real time, a three-channel flow cell is used (Hilario *et al.*, 2009). Rad51 disassembly can be measured by monitoring the decrease in the length of fluorescently end-labeled DNA onto which Rad51 is assembled. A kymograph of Rad51 disassembly is shown in Fig. 13.11C; Fig. 13.11D is the graph of DNA length versus time.

1. The syringe, tubing, and flow cell are washed at 800 μl/h with 0.5 mg/ml of BSA and 0.5 mg/ml casein in 50 m*M* Tris–HOAc (pH 7.5) at room temperature for 1 h, followed by a rinse with sample buffer for 1 h.
2. Prepare Cy3–DNA–bead complexes as described in Section 2.3.

3. Load 400 μl of solution containing Cy3–DNA–bead complexes (typically about 90 f*M*), 40 m*M* Tris–HOAc (pH 8.2), 30 m*M* DTT, and 15% (w/v) sucrose into the first channel.
4. Load 400 μl of solution containing 40 m*M* Tris–HOAc (pH 7.5), 10 m*M* $Mg(OAc)_2$, 30 m*M* DTT, and 15% (w/v) sucrose into the second channel; the ATP concentration can be varied from 0 to 2 m*M*.
5. Load 400 μl of solution containing 1 μ*M* Rad51, 40 m*M* Tris–HOAc (pH 7.5), 10 m*M* $Mg(OAc)_2$, 2 m*M* ATP, 30 m*M* DTT, and 15% (w/v) sucrose into the third channel.
6. Trap a Cy3–DNA–bead complex in the first channel.
7. Move the complex to the third channel to assemble Rad51 onto the DNA.
8. Move the complex to the second channel to initiate Rad51 disassembly from the DNA.

5.6. Visualization of $RecA^{FAM}$/RecA-RFP/$Rad51^{FAM}$ filament formation

To directly visualize nucleation (cluster formation) by fluorescent RecA or Rad51 (Galletto *et al.*, 2006; Handa *et al.*, 2009; Hilario *et al.*, 2009), a three-channel flow cell is used. To confirm that a single molecule of DNA is present, YOYO-1-stained DNA is used in the initial trapping. YOYO-1 is removed by washing the DNA in a buffer containing 5–10 m*M* $Mg(OAc)_2$ before starting the assay. A time course of RecA-RFP cluster formation is shown in Fig. 13.12. Here, we describe the protocol for imaging RecA-RFP cluster formation.

1. The syringe, tubing, and flow cell are incubated with 0.5 mg/ml of BSA in 50 m*M* Tris–HOAc (pH 7.5) at room temperature for 15 min, then rinsed with a 10-fold volume of 50 m*M* Tris–HOAc (pH 7.5).
2. Prepare YOYO-1-stained DNA–bead complexes as described in Section 2.2.
3. Load 400 μl of solution containing YOYO-1-stained DNA–bead complex, 20 m*M* Tris–HOAc (pH 8.2), 30 m*M* DTT, and 20% (w/v) sucrose into the first channel.
4. Load 400 μl of solution containing 0.5 m*M* ATPγS, 5 m*M* $Mg(OAc)_2$, 20 m*M* Tris–HOAc (pH 8.2), 30 m*M* DTT, and 20% (w/v) sucrose into the second channel.
5. Load 400 μl of solution containing RecA-RFP, 0.5 m*M* ATPγS, 1 m*M* $Mg(OAc)_2$, 20 m*M* MES (pH 6.2), 30 m*M* DTT, and 20% (w/v) sucrose into the third channel. The RecA-RFP concentration is varied from 150 to 400 n*M*.
6. Trap a YOYO-1-stained DNA–bead complex in the first channel.

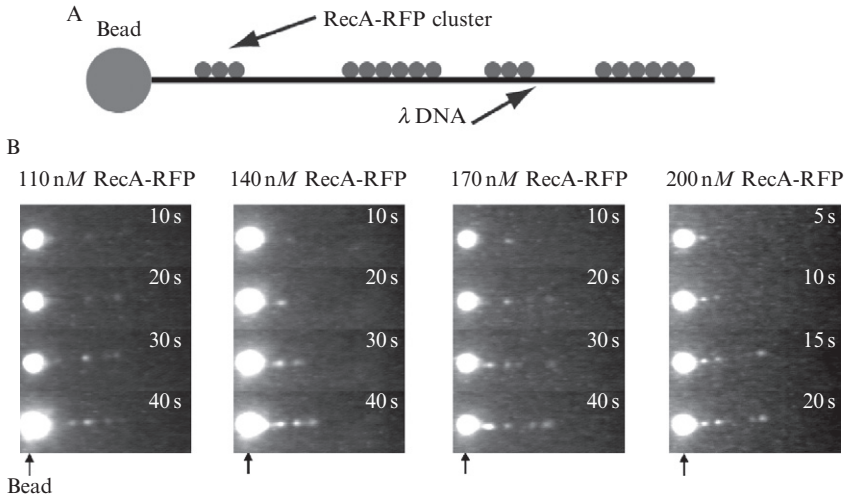

Figure 13.12 Direct visualization of nucleation and growth of RecA-RFP nucleoprotein filaments on individual molecules of dsDNA. (A) Illustration of the nucleation of RecA-RFP clusters on DNA. (B) Representative video frames showing nucleation at four different RecA-RFP concentrations. Flow is left to right. Each vertical strip represents the same DNA molecule repeatedly dipped into the RecA-RFP protein solution for the incubation times indicated. The trapped bead position is indicated by an arrow; the bead is fluorescent due to the nonspecific binding of the RecA-RFP.

7. Move the complex to the second channel to confirm by visual inspection that a single molecule of intact λ DNA is attached to the bead.
8. Incubate the complex for 2–3 min in the second channel to dissociate the YOYO-1. In this step, the shutter for excitation light is closed to avoid the photocleavage of DNA.
9. Move the complex to the third channel containing the RecA-RFP.
10. Incubate the complex for 5–30 s in the third channel. In this step, the shutter for excitation light is closed to protect the CCD camera from the strong signal due to a high concentration of fluorescent protein.
11. Move the complex to the second channel to observe the RecA-RFP clusters. To avoid the photobleaching of RecA-RFP, the illumination time should be minimized ($\sim$1–2 s).
12. Repeat steps 9 and 10.

6. Data Analysis Methods

To improve the efficiency of the single-molecule studies and increase the reliability of the data analysis, we developed programs to analyze the fluorescence images. The software is available upon request.

6.1. Two-dimensional Gaussian fitting

To determine the center of a fluorescent intensity distribution (e.g., for Cy3-end-labeled DNA or FITC–Rad54/Tid1), the distribution is fitted to the following two-dimensional Gauss function (Hilario *et al.*, 2009; Nimonkar *et al.*, 2007):

$$f(x,y) = A \times \exp\left[-\frac{(x-x_c)^2}{s_x^2} - \frac{(y-y_c)^2}{s_y^2}\right] + B \qquad (13.8)$$

Here, $f(x, y)$ is the point spread function (PSF), A the maximum intensity of PSF, x, y the coordinates of image, x_c, y_c the center of PSF, s_x, s_y the width of the PSF, and B the background intensity. To perform nonlinear regression, Eq. (13.8) is expanded to a Taylor series, and the zeroth and first derivative terms are used. The fitting process is iterated until the relative change of fitting parameters falls within a predefined threshold (5%; empirically chosen as a threshold because the fluctuation of fluorescent spot position is greater than the fluorescent spot size). To reduce the calculation time, a small region surrounding the fluorescent spot is selected for fitting. The image in the region of interest is median-filtered and averaged before fitting. The initial parameters for fitting are determined automatically from the fluorescent intensity distribution in the region. For the DNA length measurement, the radius of bead is known and subtracted from the observed length. Figs. 13.10C, 13.11B, and D show the results of a two-dimensional Gaussian fitting.

6.2. Automatic DNA length measurement

To measure the length of DNA that is either fluorescently labeled with YOYO-1 or decorated with fluorescent proteins, we developed a plug-in for ImageJ to automate the analysis. Fig. 13.9B shows an example of the analysis.

1. To improve the data quality, fluorescence images are first averaged every 5–10 frames.
2. The position of the trapped bead is initially determined manually, taking advantage of the nonspecific binding of dye to the bead.
3. For each frame, a radial line scan originating from the bead center is determined. The orientation of the DNA is determined as the direction that has the maximum mean gray value.
4. The profile along the orientation of the DNA is calculated.
5. The derivative of the profile is calculated. The position of the maximum (excluding the bead) in the derivative is the position of the DNA end. The length of the DNA is calculated as the distance from the DNA end to the bead center, minus the radius of the bead.

ACKNOWLEDGMENTS

We wish to thank Jason Bell, Aura Carreira, Petr Cejka, Anthony Forget, Joe Hilario, Taeho Kim, Hsu-Yang Lee, Katsumi Morimatsu, Amitabh Nimonkar, Behzad Rad, and Lisa Vancelette for their comments on this manuscript, and members of the Kowalczykowski lab for their contribution to this research. The research in our lab has been funded by grants from National Institutes of Health T32 CA-108459 to C. C. D., and GM-41347, GM-62653, and GM-64745 to S. C. K.

REFERENCES

Alexeev, A., Mazin, A., and Kowalczykowski, S. C. (2003). Rad54 protein possesses chromatin-remodeling activity stimulated by the Rad51-ssDNA nucleoprotein filament. *Nat. Struct. Biol.* **10,** 182–186.

Amitani, I., Baskin, R. J., and Kowalczykowski, S. C. (2006). Visualization of Rad54, a chromatin remodeling protein, translocating on single DNA molecules. *Mol. Cell* **23,** 143–148.

Anderson, D. G., and Kowalczykowski, S. C. (1997a). The recombination hot spot χ is a regulatory element that switches the polarity of DNA degradation by the RecBCD enzyme. *Genes Dev.* **11,** 571–581.

Anderson, D. G., and Kowalczykowski, S. C. (1997b). The translocating RecBCD enzyme stimulates recombination by directing RecA protein onto ssDNA in a χ-regulated manner. *Cell* **90,** 77–86.

Benson, F. E., Stasiak, A., and West, S. C. (1994). Purification and characterization of the human Rad51 protein, an analogue of E. coli RecA. *EMBO J.* **13,** 5764–5771.

Bianco, P. R., Tracy, R. B., and Kowalczykowski, S. C. (1998). DNA strand exchange proteins: A biochemical and physical comparison. *Front. Biosci.* **3,** D570–D603.

Bianco, P. R., Brewer, L. R., Corzett, M., Balhorn, R., Yeh, Y., Kowalczykowski, S. C., and Baskin, R. J. (2001). Processive translocation and DNA unwinding by individual RecBCD enzyme molecules. *Nature* **409,** 374–378.

Brewer, L. R., and Bianco, P. R. (2008). Laminar flow cells for single-molecule studies of DNA-protein interactions. *Nat. Methods* **5,** 517–525.

Campbell, M. J., and Davis, R. W. (1999). Toxic mutations in the recA gene of E. coli prevent proper chromosome segregation. *J. Mol. Biol.* **286,** 417–435.

Celliers, P. M., and Conia, J. (2000). Measurement of localized heating in the focus of an optical trap. *Appl. Opt.* **39,** 3396–3407.

Chen, Z., Yang, H., and Pavletich, N. P. (2008). Mechanism of homologous recombination from the RecA-ssDNA/dsDNA structures. *Nature* **453,** 489–494.

Conway, A. B., Lynch, T. W., Zhang, Y., Fortin, G. S., Fung, C. W., Symington, L. S., and Rice, P. A. (2004). Crystal structure of a Rad51 filament. *Nat. Struct. Mol. Biol.* **11,** 791–796.

Dillingham, M. S., and Kowalczykowski, S. C. (2008). RecBCD enzyme and the repair of double-stranded DNA breaks. *Microbiol. Mol. Biol. Rev.* **72,** 642–671.

Dixon, D. A., and Kowalczykowski, S. C. (1993). The recombination hotspot χ is a regulatory sequence that acts by attenuating the nuclease activity of the E. coli RecBCD enzyme. *Cell* **73,** 87–96.

Galletto, R., Amitani, I., Baskin, R. J., and Kowalczykowski, S. C. (2006). Direct observation of individual RecA filaments assembling on single DNA molecules. *Nature* **443,** 875–878.

Handa, N., Bianco, P. R., Baskin, R. J., and Kowalczykowski, S. C. (2005). Direct visualization of RecBCD movement reveals cotranslocation of the RecD motor after χ recognition. *Mol. Cell* **17,** 745–750.

Handa, N., Amitani, I., Gumlaw, N., Sandler, S. J., and Kowalczykowski, S. C. (2009). Single molecule analysis of a red fluorescent RecA protein reveals a defect in nucleoprotein filament nucleation that relates to its reduced biological functions. *J. Biol. Chem.* **284,** 18664–18673.

Hilario, J., Amitani, I., Baskin, R. J., and Kowalczykowski, S. C. (2009). Direct imaging of human Rad51 nucleoprotein dynamics on individual DNA molecules. *Proc. Natl. Acad. Sci. USA* **106,** 361–368.

Holzen, T. M., Shah, P. P., Olivares, H. A., and Bishop, D. K. (2006). Tid1/Rdh54 promotes dissociation of Dmc1 from nonrecombinogenic sites on meiotic chromatin. *Genes Dev.* **20,** 2593–2604.

Karstens, T., and Kobs, K. (1980). Rhodamine-B and rhodamine-101 as reference substances for fluorescence quantum yield measurements. *J. Phys. Chem.* **84,** 1871–1872.

Kato, H., Nishizaka, T., Iga, T., Kinosita, K. Jr., and Ishiwata, S. (1999). Imaging of thermal activation of actomyosin motors. *Proc. Natl. Acad. Sci. USA* **96,** 9602–9606.

Klein, H. L. (1997). RDH54, a RAD54 homologue in Saccharomyces cerevisiae, is required for mitotic diploid-specific recombination and repair and for meiosis. *Genetics* **147,** 1533–1543.

Kowalczykowski, S. C. (2000). Initiation of genetic recombination and recombination-dependent replication. *Trends Biochem. Sci.* **25,** 156–165.

Liu, Y., Cheng, D. K., Sonek, G. J., Berns, M. W., Chapman, C. F., and Tromberg, B. J. (1995). Evidence for localized cell heating induced by infrared optical tweezers. *Biophys. J.* **68,** 2137–2144.

Mao, H., Arias-Gonzalez, J. R., Smith, S. B., Tinoco, I. Jr., and Bustamante, C. (2005). Temperature control methods in a laser tweezers system. *Biophys. J.* **89,** 1308–1316.

Mazin, A. V., Bornarth, C. J., Solinger, J. A., Heyer, W. D., and Kowalczykowski, S. C. (2000). Rad54 protein is targeted to pairing loci by the Rad51 nucleoprotein filament. *Mol. Cell* **6,** 583–592.

Mazin, A. V., Alexeev, A. A., and Kowalczykowski, S. C. (2003). A novel function of Rad54 protein: Stabilization of the Rad51 nucleoprotein filament. *J. Biol. Chem.* **278,** 14029–14036.

Modesti, M., Ristic, D., van der Heijden, T., Dekker, C., van Mameren, J., Peterman, E. J., Wuite, G. J., Kanaar, R., and Wyman, C. (2007). Fluorescent human RAD51 reveals multiple nucleation sites and filament segments tightly associated along a single DNA molecule. *Structure* **15,** 599–609.

Neuman, K. C., and Block, S. M. (2004). Optical trapping. *Rev. Sci. Instrum.* **75,** 2787–2809.

Nimonkar, A. V., Amitani, I., Baskin, R. J., and Kowalczykowski, S. C. (2007). Single molecule imaging of Tid1/Rdh54, a Rad54 homolog that translocates on duplex DNA and can disrupt joint molecules. *J. Biol. Chem.* **282,** 30776–30784.

Ogawa, T., Yu, X., Shinohara, A., and Egelman, E. H. (1993). Similarity of the yeast RAD51 filament to the bacterial RecA filament. *Science* **259,** 1896–1899.

Peterman, E. J. G., Gittes, F., and Schmidt, C. F. (2003). Laser-induced heating in optical traps. *Biophys. J.* **84,** 1308–1316.

Petukhova, G., Stratton, S., and Sung, P. (1998). Catalysis of homologous DNA pairing by yeast Rad51 and Rad54 proteins. *Nature* **393,** 91–94.

Prasad, T. K., Yeykal, C. C., and Greene, E. C. (2006). Visualizing the assembly of human Rad51 filaments on double-stranded DNA. *J. Mol. Biol.* **363,** 713–728.

Prasad, T. K., Robertson, R. B., Visnapuu, M. L., Chi, P., Sung, P., and Greene, E. C. (2007). A DNA-translocating Snf2 molecular motor: Saccharomyces cerevisiae Rdh54 displays processive translocation and extrudes DNA loops. *J. Mol. Biol.* **369,** 940–953.

Robertson, R. B., Moses, D. N., Kwon, Y., Chan, P., Chi, P., Klein, H., Sung, P., and Greene, E. C. (2009). Structural transitions within human Rad51 nucleoprotein filaments. *Proc. Natl. Acad. Sci. USA* **106,** 12688–12693.

Roman, L. J., and Kowalczykowski, S. C. (1989). Characterization of the helicase activity of the *Escherichia coli* RecBCD enzyme using a novel helicase assay. *Biochemistry* **28,** 2863–2873.

Romano, V., Zweig, A. D., Frenz, M., and Weber, H. P. (1989). Time-resolved thermal microscopy with fluorescent films. *Appl. Phys. B Photophys. Laser Chem.* **49,** 527–533.

Schatz, P. J. (1993). Use of peptide libraries to map the substrate specificity of a peptide-modifying enzyme: A 13 residue consensus peptide specifies biotinylation in *Escherichia coli*. *Biotechnology (N. Y.)* **11,** 1138–1143.

Shinohara, M., Shita-Yamaguchi, E., Buerstedde, J. M., Shinagawa, H., Ogawa, H., and Shinohara, A. (1997). Characterization of the roles of the *Saccharomyces cerevisiae* RAD54 gene and a homologue of RAD54, RDH54/TID1, in mitosis and meiosis. *Genetics* **147,** 1545–1556.

Shinohara, M., Gasior, S. L., Bishop, D. K., and Shinohara, A. (2000). Tid1/Rdh54 promotes colocalization of rad51 and dmc1 during meiotic recombination. *Proc. Natl. Acad. Sci. USA* **97,** 10814–10819.

Solinger, J. A., and Heyer, W. D. (2001). Rad54 protein stimulates the postsynaptic phase of Rad51 protein-mediated DNA strand exchange. *Proc. Natl. Acad. Sci. USA* **98,** 8447–8453.

Solinger, J. A., Lutz, G., Sugiyama, T., Kowalczykowski, S. C., and Heyer, W. D. (2001). Rad54 protein stimulates heteroduplex DNA formation in the synaptic phase of DNA strand exchange via specific interactions with the presynaptic Rad51 nucleoprotein filament. *J. Mol. Biol.* **307,** 1207–1221.

Solinger, J. A., Kiianitsa, K., and Heyer, W. D. (2002). Rad54, a Swi2/Snf2-like recombinational repair protein, disassembles Rad51:dsDNA filaments. *Mol. Cell* **10,** 1175–1188.

Spies, M., and Kowalczykowski, S. C. (2005). Homologous recombination by RecBCD and RecF pathways. *In* "The Bacterial Chromosome," (N. P. Higgins, ed.), pp. 389–403. ASM Press, Washington, DC.

Spies, M., Bianco, P. R., Dillingham, M. S., Handa, N., Baskin, R. J., and Kowalczykowski, S. C. (2003). A molecular throttle: The recombination hotspot χ controls DNA translocation by the RecBCD helicase. *Cell* **114,** 647–654.

Spies, M., Amitani, I., Baskin, R. J., and Kowalczykowski, S. C. (2007). RecBCD enzyme switches lead motor subunits in response to χ recognition. *Cell* **131,** 694–705.

Stasiak, A., Di Capua, E., and Koller, T. (1981). Elongation of duplex DNA by recA protein. *J. Mol. Biol.* **151,** 557–564.

Sung, P., and Robberson, D. L. (1995). DNA strand exchange mediated by a RAD51-ssDNA nucleoprotein filament with polarity opposite to that of RecA. *Cell* **82,** 453–461.

Taylor, A. F., and Smith, G. R. (1995). Strand specificity of nicking of DNA at Chi sites by RecBCD enzyme: Modulation by ATP and magnesium levels. *J. Biol. Chem.* **270,** 24459–24467.

van der Heijden, T., Seidel, R., Modesti, M., Kanaar, R., Wyman, C., and Dekker, C. (2007). Real-time assembly and disassembly of human RAD51 filaments on individual DNA molecules. *Nucleic Acids Res.* **35,** 5646–5657.

Zaitsev, E. N., and Kowalczykowski, S. C. (2000). A novel pairing process promoted by *Escherichia coli* RecA protein: Inverse DNA and RNA strand exchange. *Genes Dev.* **14,** 740–749.